NAVAL POSTGRADUATE SCHOOL

MONTEREY, CALIFORNIA

THESIS

WAVE REFLECTION ON A TWO-SLOPE STEEP BEACH

by

David H. Watson

March 2012

Thesis Advisor: Jamie MacMahan
Second Reader: Thomas Herbers

Approved for public release: distribution is unlimited

THIS PAGE INTENTIONALLY LEFT BLANK

REPORT DOCUMENTATION PAGE			*Form Approved OMB No. 0704-0188*
Public reporting burden for this collection of information is estimated to average 1 hour per response, including the time for reviewing instruction, searching existing data sources, gathering and maintaining the data needed, and completing and reviewing the collection of information. Send comments regarding this burden estimate or any other aspect of this collection of information, including suggestions for reducing this burden, to Washington headquarters Services, Directorate for Information Operations and Reports, 1215 Jefferson Davis Highway, Suite 1204, Arlington, VA 22202-4302, and to the Office of Management and Budget, Paperwork Reduction Project (0704-0188) Washington DC 20503.			
1. AGENCY USE ONLY ***(Leave blank)***	**2. REPORT DATE** March 2012	**3. REPORT TYPE AND DATES COVERED** Master's Thesis	
4. TITLE AND SUBTITLE Wave Reflection on a Two-Slope Steep Beach			**5. FUNDING NUMBERS**
6. AUTHOR(S) David H. Watson			
7. PERFORMING ORGANIZATION NAME(S) AND ADDRESS(ES) Naval Postgraduate School Monterey, CA 93943-5000			**8. PERFORMING ORGANIZATION REPORT NUMBER**
9. SPONSORING /MONITORING AGENCY NAME(S) AND ADDRESS(ES) N/A			**10. SPONSORING/MONITORING AGENCY REPORT NUMBER**
11. SUPPLEMENTARY NOTES The views expressed in this thesis are those of the author and do not reflect the official policy or position of the Department of Defense or the U.S. Government. IRB Protocol number _____N/A_____.			
12a. DISTRIBUTION / AVAILABILITY STATEMENT Approved for public release: distribution is unlimited			**12b. DISTRIBUTION CODE** A

13. ABSTRACT (maximum 200 words)

Wave reflection of sea-swell (0.05–0.20 Hz) energy on a two-slope (1/7.6 nearshore and 1/19 offshore) steep beach with no subaqueous sandbar is studied. The dataset were collected using a cross-shore array of 4 Acoustic Doppler Current Profilers measuring velocity and pressure at 1 Hz continuously for 40 days. Measurement of pressure and velocity at the same location allows data to be decomposed into onshore and offshore components to determine reflection. The long data set captured a wide range of wave conditions at various tidal stages. Observations show low amplitude long period waves produced energy reflection coefficients up to 80%, with most in the 30–50% range. There was a measured increase in the number of nodes and anti-nodes at higher frequencies and observations farther offshore consistent with theory. Field data were compared to an analytical two-slope model that predicts the cross-shore nodal structure of standing waves. The predicted locations of nodes and anti-nodes are in good agreement with observations.

14. SUBJECT TERMS Wave Reflection			**15. NUMBER OF PAGES** 49
			16. PRICE CODE
17. SECURITY CLASSIFICATION OF REPORT Unclassified	**18. SECURITY CLASSIFICATION OF THIS PAGE** Unclassified	**19. SECURITY CLASSIFICATION OF ABSTRACT** Unclassified	**20. LIMITATION OF ABSTRACT** UU

NSN 7540-01-280-5500 Standard Form 298 (Rev. 2-89)
Prescribed by ANSI Std. 239-18

THIS PAGE INTENTIONALLY LEFT BLANK

Approved for public release: distribution is unlimited

WAVE REFLECTION ON A TWO-SLOPE STEEP BEACH

David H. Watson
Lieutenant, United States Navy
B.S., University of Maryland University College, 2005

Submitted in partial fulfillment of the
requirements for the degree of

MASTER OF SCIENCE IN METEOROLOGY AND PHYSICAL OCEANOGRAPHY

from the

NAVAL POSTGRADUATE SCHOOL
March 2012

Author: David Watson

Approved by: Jamie MacMahan
Thesis Advisor

Thomas Herbers
Second Reader

Jeffrey D. Paduan
Chair, Department of Oceanography

THIS PAGE INTENTIONALLY LEFT BLANK

ABSTRACT

Wave reflection of sea-swell (0.05–0.20 Hz) energy on a two-slope (1/7.6 nearshore and 1/19 offshore) steep beach with no subaqueous sandbar is studied. The dataset were collected using a cross-shore array of 4 Acoustic Doppler Current Profilers measuring velocity and pressure at 1 Hz continuously for 40 days. Measurement of pressure and velocity at the same location allows data to be decomposed into onshore and offshore components to determine reflection. The long data set captured a wide range of wave conditions at various tidal stages. Observations show low amplitude long period waves produced energy reflection coefficients up to 80%, with most in the 30–50% range. There was a measured increase in the number of nodes and anti-nodes at higher frequencies and observations farther offshore consistent with theory. Field data were compared to an analytical two-slope model that predicts the cross-shore nodal structure of standing waves. The predicted locations of nodes and anti-nodes are in good agreement with observations.

THIS PAGE INTENTIONALLY LEFT BLANK

TABLE OF CONTENTS

I. INTRODUCTION....1

II. FIELD EXPERIMENT....11
- **A. LOCATION....11**
- **B. EQUIPMENT....13**

III. METHODOLOGY....15

IV. MODEL COMPARISON....21
- **A. MODEL OVERVIEW....21**
- **B. MODEL VALIDATION....26**

V. SUMMARY AND CONCLUSION....29

LIST OF REFERENCES....31

INITIAL DISTRIBUTION LIST....33

THIS PAGE INTENTIONALLY LEFT BLANK

LIST OF FIGURES

Figure 1. The four breaker types and typical values of ξ. 2

Figure 2. Battjes reflection parameter (R) plotted against ξ for multiple beach slopes. (From: Ching-Piao Tsai et al., (2002))....4

Figure 3. Beach profile and sensor location at El Moreno Beach (From Suhayda, 1974) 5

Figure 4. (A) Beach profile for (After: Elgar et al. (1994) Duck NC), (B) (After: Miles and Russell (2004) Teignmouth, UK.)....7

Figure 5. Carmel River State Beach located in Carmel, CA, viewed facing west into the Carmel Valley. 11

Figure 6. Cross-shore profile of Carmel River Beach, CA, derived from surveys taken during cross-shore transport study experiment. 12

Figure 7. Sea kayak with echo sounder and Ashtech z-Xtreme GPS attached. An Ashtech z-Xtreme GPS mounted in a backpack used for beach surveys. 13

Figure 8. Top-down view of instrument array used for the experiment at CRSB, Carmel, CA. Green boxes indicate ADCP locations. 14

Figure 9. Hourly tide (A), wave height (B), and period (C) at CRSB. 16

Figure 10. Hourly energy density spectra of onshore wave energy as a function of frequency and yearday. Energy color scale is plotted to the right. 17

Figure 11. Measured nodal structure averaged by frequency for tides. 18

Figure 12. A) R^2 as a function of H (m) and T (s), where colors represent R^2 values. B) R^2 as a function of tides. Dashed line represents linear regression for T_{mo} (wave period)<11. C) Battjes (1974) equation solved for beach slope, where colors represent T_{mo} 19

Figure 13. Quad panel of averaged onshore energy density (upper panel) and averaged R^2 in frequency for sensors 1–4....20

Figure 14. Coordinate system for a one-slope beach. 22

Figure 15. Coordinate system for a two-slope beach. 24

Figure 16. Measured (dashed black) versus predicted (red) nodal structure of reflected wave energy in the sea-swell frequency band for sensors 1–4. Top panel is high tide, center is MSL, and bottom is low tide. 26

Figure 17. Predicted frequency spectra in sea swell frequency band in the cross-shore. Inset is measured nodal structure averaged over tides. Red vertical lines indicate sensor locations the white line marks the slope break. Warmer colors correspond to anti-nodes. 27

THIS PAGE INTENTIONALLY LEFT BLANK

LIST OF ACRONYMS AND ABBREVIATIONS

ADCP	Acoustic Data Current Profiler
AWAC	Acoustic Wave and Current Profiler
CRSB	Carmel River State Beach
h	Water Depth
H	Wave Height
H_c	Critical Height for Wave Breaking
H_r	Reflected Wave Height
Hz	Hertz
g	Gravity
GPS	Global Position System
L_0	Deepwater Wavelength
J_0	Zero Order Bessel Function
R	Refection
T	Wave Period
x	Cross-Shore Distance
x_{sb}	Cross-Shore Location of Slope Break
β	Beach Slope
ξ	Surf Similarity Parameter

THIS PAGE INTENTIONALLY LEFT BLANK

ACKNOWLEDGMENTS

This thesis would not have been possible without the guidance of my advisor Professor Jamie MacMahan. His love of oceanography inspires students to learn all they can from him and is exactly why I asked him to be my advisor. I appreciate how Professor MacMahan includes his students in the complete process of a thesis project. Beginning with researching and setting up the experiment, collecting the data in the field then analyzing the results. During the field experiment I was blown away by the professionalism and outstanding support provided by Ron Cowen and Keith Wyckoff. Mike Cook was single handedly responsible for enabling me to translate Professor MacMahan's ideas into a functional model crucial to my thesis. Without his efforts this would not have been possible. PHD students Jenna Brown and LCDR Micah Weltmer were always willing to assist by answering my frequent questions. They are both unbelievable assets to the Oceanography department at Naval Postgraduate School. Last but not least I would like to thank my family for putting up with me during this whole process. With their full support and encouragement anything is possible.

THIS PAGE INTENTIONALLY LEFT BLANK

I. INTRODUCTION

Energy from distant storms propagates toward coasts as sea-swell waves, which can dissipate, partially reflect, or fully reflect. Miche (1951) empirically determined that the amount of reflection depends on the amount of onshore wave energy that is lost to dissipation when waves break. Battjes (1974) showed that reflection and dissipation are a function of beach slope, wave height and wave period. Dissipative beaches are associated with spilling waves on gentle slopes; in contrast, on steep beaches long low waves, tend not to break and instead surge up the beach with large amounts of onshore wave energy available for reflection.

As waves move onshore into shallow water they shoal, causing waves to steepen. The slope of the beach (β) and wave steepness, defined as $(H/L)$where H is wave height and L is wavelength determine where, or if, wave breaking will occur. Dissipative waves tend to break farther offshore as a result of gradual slopes and steeper waves. Spilling and plunging waves are classified as dissipative. Reflective waves include collapsing and surging, which are low waves with longer periods that break close to shore, or not at all due to the steeper slopes. To determine breaker type Iribarren and Nogales (1949) developed the surf similarity parameter (ξ). ξ evaluates the relationship between (β) and the steepness of the wave, defined as H/L_0 where L_0 is deepwater wavelength to determine the breaker type given a specific beach slope and wave steepness:

$$\xi = \tan\beta / \sqrt{H/L_0}\ . \qquad (1)$$

A value < 3 is classified as breaking and associated with dissipative beaches whereas $\xi \geq 3$ is classified as non-breaking and associated with reflective beaches (Figure 1).

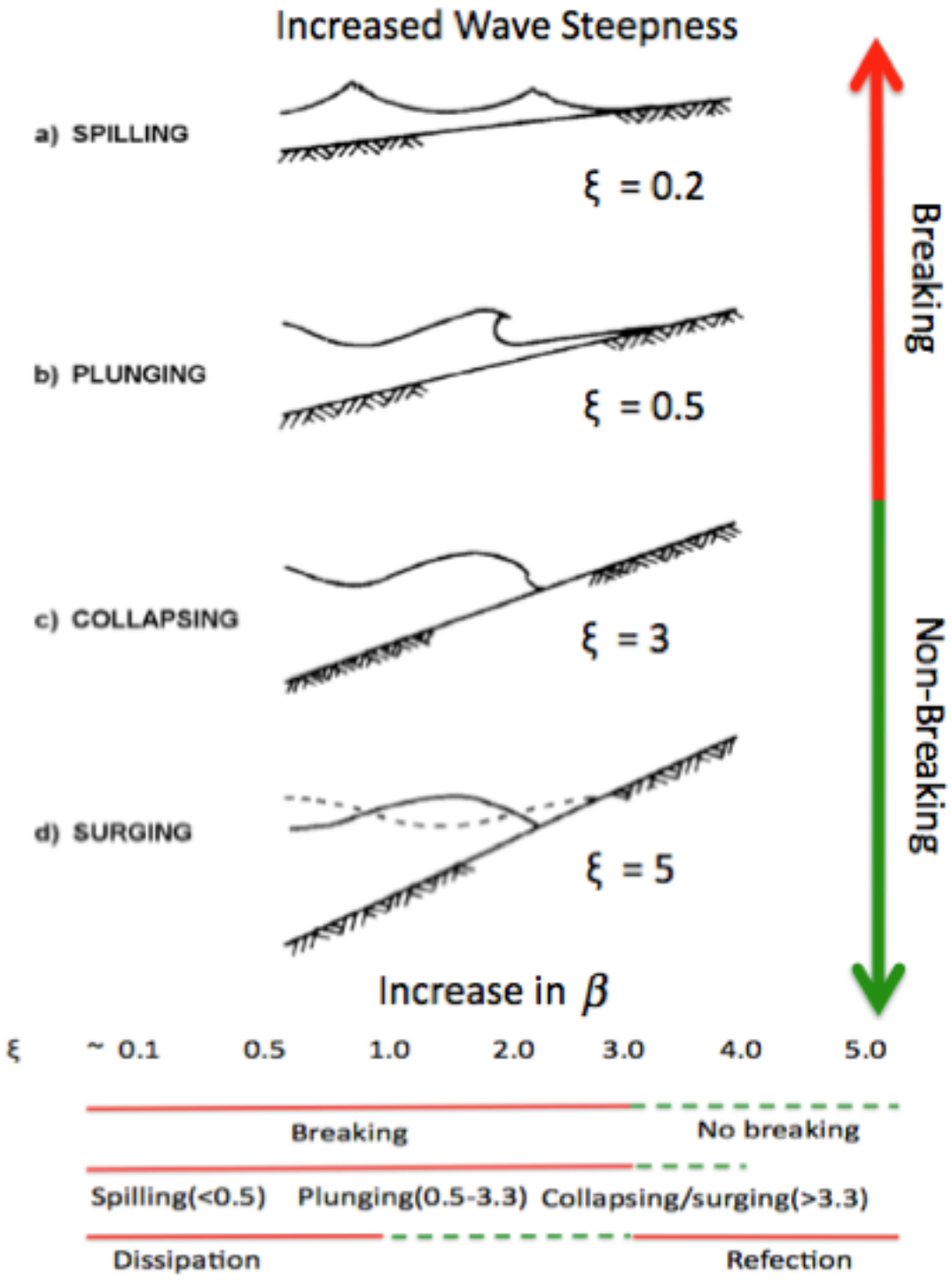

Figure 1. The four breaker types and typical values of ξ.

Battjes (1974) realizing that the amount of reflected energy was dependent on the amount of energy lost to dissipation redefined Miche's (1951) theory of reflection utilizing the ξ. Miche (1951) defined reflection as

$$R = \left(H_0 / L_0\right)_c / \left(H_0 / L_0\right), \tag{2}$$

which is the ratio of critical steepness, or the steepest wave before breaking occurs $\left(H_0 / L_0\right)_c$ to the observed wave steepness $\left(H_0 / L_0\right)$. Battjes (1974) redefined R by substituting ξ for wave steepness. His expression for reflection is

$$R = 0.1\xi^2, \tag{3}$$

for $\xi < 3$, which represents the ratio of the wave amplitude (H) propagating offshore to the onshore, wave amplitude. Note R^2 discussed later represents the ratio of energy (H^2) for offshore to onshore where $R = \sqrt{R^2}$. The term offshore is used to describe wave energy reflected from the beach moving back out to sea.

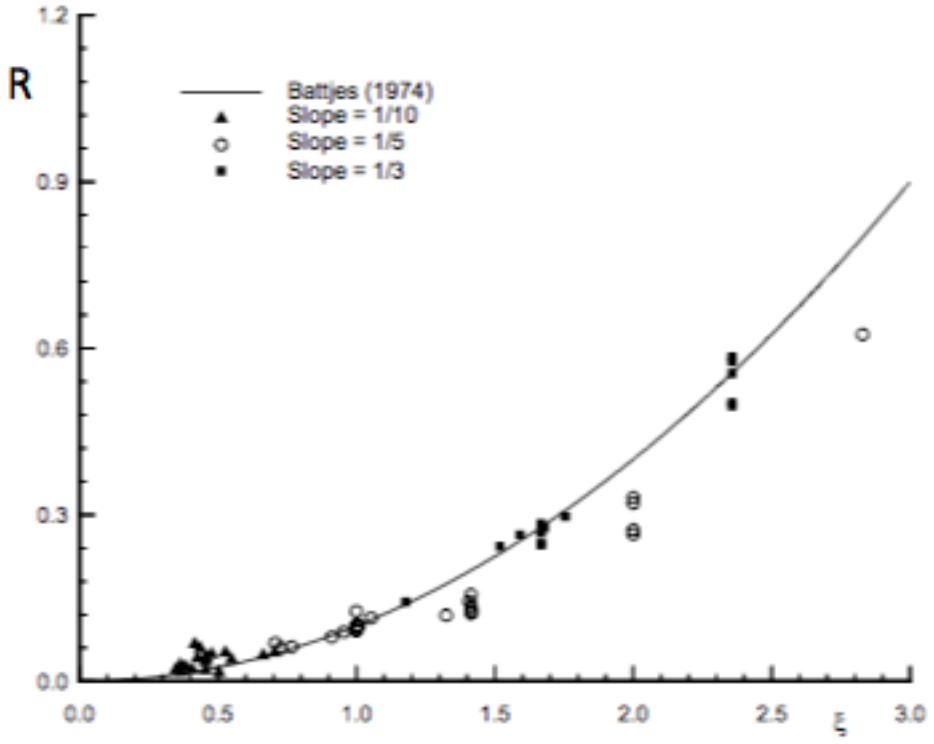

Figure 2. Battjes reflection parameter (R) plotted against ξ for multiple beach slopes. (From: Ching-Piao Tsai et al., (2002))

While evaluating several empirical formulas for wave shoaling and breaking on steep slopes Ching-Piao Tsai et al. validated the Battjes (1974) reflection parameter in 2002. They evaluated R against ξ on three steep slopes of 1/3, 1/5, and 1/10 using a wave channel to empirically validate Battjes (1974) expression (Figure. 2). They found that the Battjes (1974) expression works well for monochromatic waves on planar slopes.

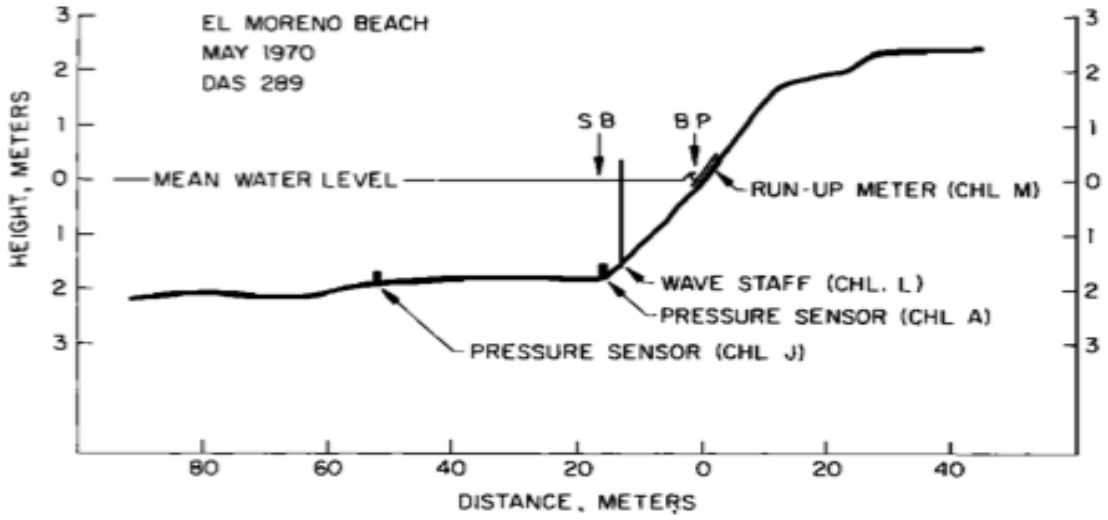

Figure 3. Beach profile and sensor location at El Moreno Beach (From Suhayda, 1974)

Natural beaches are composed of complicated slopes and encounter a wide spectrum of wave frequencies, amplitudes, and directions. Suhayda (1974) conducted a field experiment investigating standing waves on a natural beach. He expanded on the theoretical results of Lamb (1932), Friedrichs (1948), Carrier and Greenspan (1958), and Carrier (1966) as well as experimental studies of wave reflection by Taira and Nagata (1968) by collecting and analyzing field data to validate expressions to predict cross-shore nodal structure. His beach, which was located on the west coast of the Gulf of California where low steepness swell frequently occurs, was composed of a smooth nearshore slope (1/7) and a very gentle offshore slope of (1/500) with the slope break at 15.3m offshore (Figure 3). The combination of the steep nearshore slope and low steepness swell were ideal for the formation of reflective waves. Analyzing four sets of data collected in 20 minute records confirmed that swell energy was strongly reflected with reflection coefficient (Miche (1951)) of ~ 0.7. The reflected energy was observed to produce standing waves. Suhayda (1974) proved that waves were reflecting nearly perpendicular to the beach +/- 5° causing a potential shift in the nodes/antinodes of <1°. Since the angular approach of waves to the beach could be ignored, he utilized a two-dimensional model to predict cross-shore nodal structure on a beach composed of two

slopes. Sea surface elevation (n) is expressed at the nearshore slope ($0 < x < x_{sb}$) as a function of frequency by,

$$n_1(x,t) = \int s(\sigma) J_0 \left[\frac{\sqrt{2\sigma x}}{\sqrt{(g \tan \beta)}} \right] e^{i(\sigma t + \in)}, \quad (4)$$

where $S(\sigma)$ is wave amplitude, J_0 represents a zero order Bessel Function, $\sigma = 2\pi / T$ where T is wave period, x is the cross-shore distance, g is gravity, x_{sb} is the location of the slope break and $\in$ is phase. Seaward of the slope break ($x_{sb} < x < \infty$) is expressed as a function of frequency by

$$n_2(x,t) = \left[\int A(\sigma) \sin \frac{2\pi}{L} x + B(\sigma) \cos \frac{2\pi}{L} x \right] e^{i(\sigma t + \in)} \partial\sigma, \quad (5)$$

where A and B represent amplitudes of the σ component and L is the wavelength in shallow water. To accurately predict wave behavior, the solutions for equations 4 and 5 were matched at the slope break. Results indicated that the predicted locations of nodes/anti-nodes were in good agreement with measured data.

Hotta et al. (1981) analyzed field data to study onshore and reflected wave energy utilizing the Suhayda (1974) equations. Observed data indicated nearshore onshore long wave energy was reflected leading to the formation of standing waves. The model used by Hotta et al. (1981) was configured to resolve wave behavior on a two-slope beach utilizing sea surface heights and on-offshore velocity. Data were collected primarily at two beaches during the experiment. The first beach had a β of 1/60–1/70 with a subaqueous sand bar. The second more reflective beach was composed of two-slopes with a steep nearshore β of 1/10 and a gentler 1/50 offshore. Unfortunately the two data sets collected on these beaches were only 2 hrs and 12 minutes respectively. The short duration of the data set does not allow changes in reflection due to varied wave and tidal conditions to be studied.

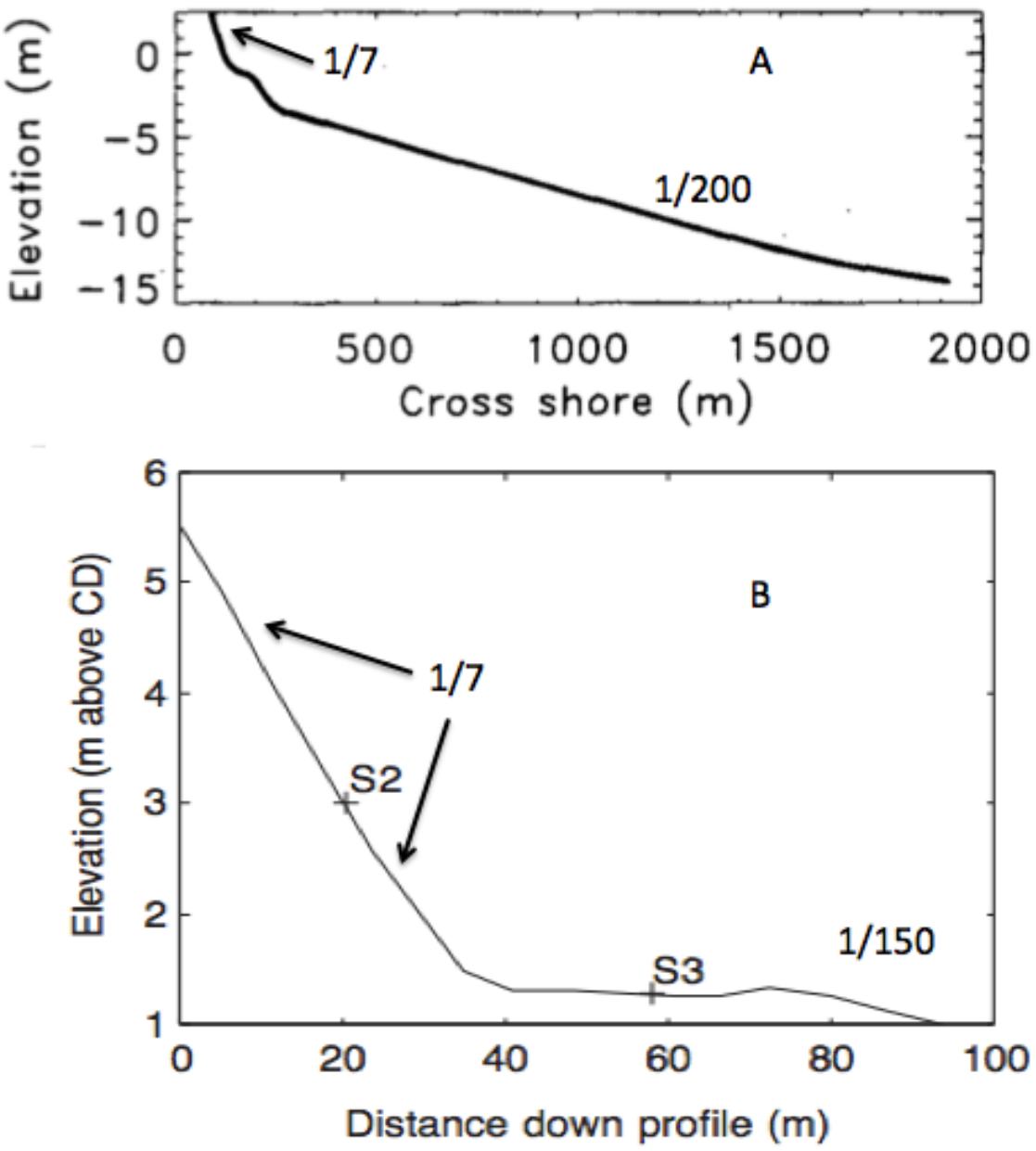

Figure 4. (A) Beach profile for (After: Elgar et al. (1994) Duck NC), (B) (After: Miles and Russell (2004) Teignmouth, UK.)

There have been few studies of wave reflection in nature. Elgar et al. (1994) conducted a field study of wave reflection at Duck, North Carolina (Figure 4A). The beach is composed of a sandy seafloor with a gradual slope of 1/200 at the location of the sensors used to measure data. However, during high tide a steep beach face of 1/7 is

available to reflect wave energy. Dissipation is also increased by the presence of a subaqueous bar in 1.5 meters of water. During high tide, maximum R^2 values of 18% were measured when the sand bar was at its deepest and the steep nearshore slope was submerged. Highest values were observed when longer period lower amplitude waves were present. Results of frequency-directional spectra showed specular reflection in the sea-swell energy band. Although the Elgar et al. (1994) field experiment contains a large data set, the gentle slope of the beach and presence of a sand bar introduced multiple reflectors and dissipaters.

Miles and Russell (2004) conducted an experiment at Teignmouth beach on the east coast of the UK to investigate surf zone hydrodynamics and sediment transport on a two-slope beach (Figure 4B) with bimodal sediment composition. The upper beach with a steep slope (1/7) is composed of course sand while the low tide terrace with a gentle slope (1/150) is composed of fine sand. A large mean tidal range at the beach of 4.2 m allows for both reflective and dissipative characteristics at the same location. Results showed reflection coefficients of ~ 45% on the upper slope versus ~ 30% on the lower terrace. Results confirm that both reflective and dissipative characteristics are present on the same beach in receipt of the same onshore wave energy, relative to tides.

For this thesis, a 40-day field study was performed on a two-slope steep beach with no subaqueous bar in Carmel, CA. The nearshore slope is 1/7.6 and the outer slope is 1/19 resulting in a highly reflective beach regardless of tide. The beach routinely receives long period, low amplitude sea-swell waves and is protected from the west to northwest. Acoustic Data Current Profilers (ADCP) that measure cross-shore velocity and pressure were positioned at four locations along the outer slope in a line array. Measuring velocity and pressure at the same location allows wave energy to be decomposed into onshore and offshore components (Sheremet et al., 2002). The length of the dataset captured a wide spectrum of wave conditions over all tidal stages. The field results were utilized to validate the analytical 2-slope model from Hotta et al. (1981). Validation of this model is important to develop a better understanding of wave reflection in order to predict changes to coastline structure due to sediment transport. Reflection from natural beaches is still poorly understood due to the relatively small

number of field studies. This research will lead to a better understanding of the nearshore environment, which is vital to characterizing the battle space for naval operations. The ability to predict beach slope based on observed wave structure would be an asset to commanders in charge of amphibious operations, where bathymetry is unavailable or unreliable.

THIS PAGE INTENTIONALLY LEFT BLANK

II. FIELD EXPERIMENT

A. LOCATION

Figure 5. Carmel River State Beach located in Carmel, CA, viewed facing west into the Carmel Valley.

Wave data were collected over a 40-day period as part of a cross-shore sediment transport study conducted from June to July 2011 at Carmel River State Beach (CRSB), CA, located approximately 5 miles south of Monterey, CA, on Carmel Bay in Central California (Figure 5). CRSB is a concave beach that acts as a barrier beach for the Carmel River and is approximately 500m in length and composed of two-slopes (Figure 6) with no subaqueous sand bar. The experiment was conducted immediately north of the Carmel River outlet. The Carmel River is an ephemeral river that empties into the bay only when the lagoon floods due to high discharge from seasonal rains or when waves overtop the barrier during winter storms (Laudier et al., 2009). When the lagoon breaches, rocks and gravel from the river are discharged to the bay. The beach is composed of materials carried by the river.

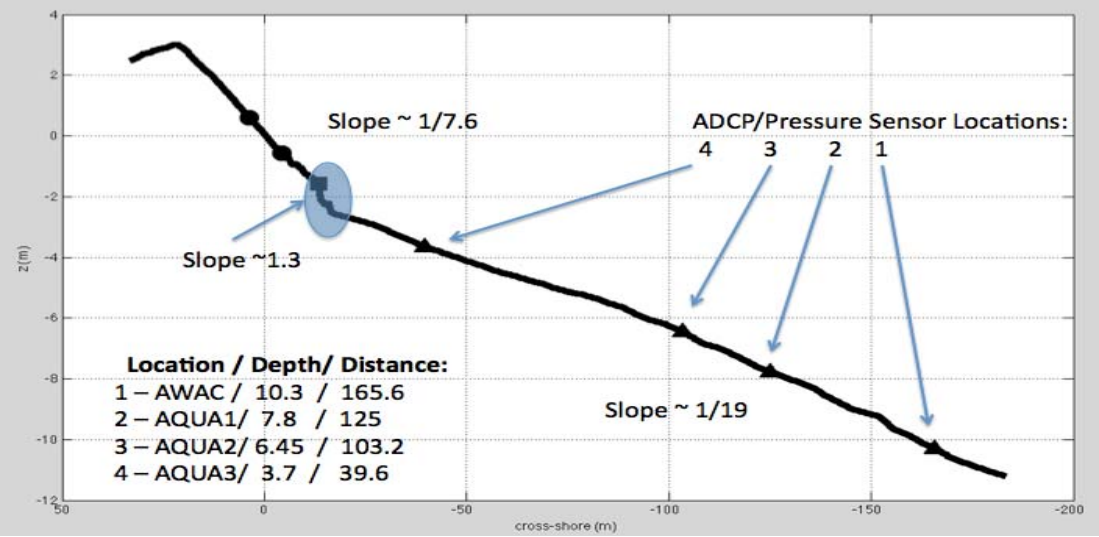

Figure 6. Cross-shore profile of Carmel River Beach, CA, derived from surveys taken during cross-shore transport study experiment.

Starting from the shoreline and moving offshore, the beach extends 20m seaward at a steep slope of 1/7.6 and terminates in a very steep, but short, step with a slope of 1/3 and roughly 0.5m in width. Seaward of the step the angle shallows to 1/19 as it continues out into the Monterey Bay (Figure 6). The beach is composed of medium to coarse sands and pebbles except at the step, which is composed of medium to large size rocks based on observations made by divers during the experiment. The beach is composed of discharge from the Carmel River and small pieces of rock from reefs to the south and headland to the north (Laudier et al., 2009). Finer materials are carried out to sea. Due to the steep angle of the slope, this beach primarily encounters surging or collapsing type waves building a steep, high berm. The coarse sand and the steep slope create a beach absent of a sand bar. The absence of the sandbar, length of the data set collected, and steepness of both slopes are features unique to this experiment.

The reef to the south and headland to the north protect the beach from waves arriving from the west to northwest. Most wave energy arriving at the beach has been reduced to swell energy from distant storms entering through a narrow opening between the headlands. The orientation of the beach also causes most incident wave energy to arrive normal to the beach.

B. EQUIPMENT

Beach and subaqueous surveys were taken daily during the experiment. Surveys were conducted using an Ashtech Z-Xtreme survey grade GPS system, which has a horizontal accuracy of 1 cm and vertical accuracy of 2 cm. Surveys of the beach were comprised of lines spaced ~ 20 m. Subaqueous surveys were completed using an echo sounder and an Ashtech Z-Xtreme GPS System mounted to a sea kayak. Beach surveys were walked during the experiment with instruments carried in a backpack (Figure 7).

Figure 7. Sea kayak with echo sounder and Ashtech z-Xtreme GPS attached. An Ashtech z-Xtreme GPS mounted in a backpack used for beach surveys.

Four Nortek Acoustic Doppler Current Profilers (ADCP) measured horizontal velocity and pressure at 1 Hz. ADCP were arranged in a cross-shore line array and configured to measure cross-shore velocity normal to the beach (Figure 8). The sensors ability to measure velocity and pressure at one location enables the data to be decomposed into incoming and outgoing components using a procedure discussed in chapter 3. Sensor location 1 was located 165.6m from shore at a depth of 10.3m.

Sensor location 2 was located 125m from shore at a depth 7.8m. Sensor location 3 was located 103.2m from shore at a depth of 6.45m. Sensor location 4 was located 39.6m from shore at depth of 3.7m (Figure 6).

Figure 8. Top-down view of instrument array used for the experiment at CRSB, Carmel, CA. Green boxes indicate ADCP locations.

III. METHODOLOGY

The pressure (p) and cross-shore velocity (u) data are decomposed into onshore (+) and offshore (-) energy components, for long waves, utilizing the general solution to allow for all frequencies to be estimated, defined by,

$$E(f,x)\pm = \frac{1}{4}\left\{ Co_{pp}\left[\frac{\cosh(Kh)}{\cosh(Kdp)}\right]^2 \pm Co_{uu}\left[\frac{\sigma}{gK}\frac{\cosh(Kh)}{\cosh(Kdu)}\right]^2 \pm \frac{1}{2}Co_{pu}\left[\frac{\sigma}{gK}\frac{\cosh^2(Kh)}{\cosh(Kdp)\cosh(Kdu)}\right]\right\} \quad (7)$$

where Co_{pp} and Co_{uu} are the auto spectra of p and u respectively and Co_{pu} is the co-spectrum of p and u. Eq. 8 is based on previous work by Sheremet et al. (2002). K is wave number, du is height of the velocity sensor from the bed, and dp is height of the pressure sensor from the bed. Data is converted to sea surface heights in this case using a transformation function indicated by [ ]. The first and second terms represent pressure (potential) and velocity (kinetic) contributions to the energy. The third term describes the difference between in phase (shoreward) and 180° out of phase out of phase (seaward) energy contribution. The noise floor, calculated by taking the average of a few frequency bands near the Nyquist frequency is removed from the first two terms. The third term does not contain noise as it only describes the coherent part of the pressure and velocity field. Reflection is expressed as a ratio of outgoing to incoming and wave energy components using,

$$R^2(f) = \frac{E(f)-}{E(F)+}. \quad (8)$$

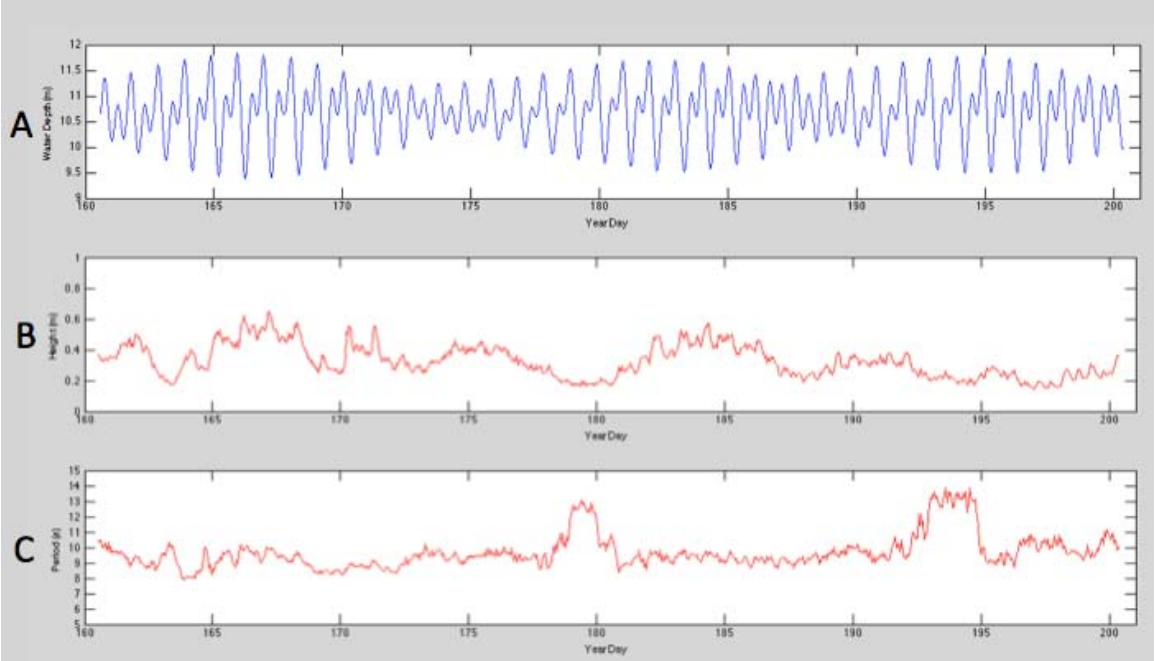

Figure 9. Hourly tide (A), wave height (B), and period (C) at CRSB.

CRSB is a mixed tide environment (Figure 9A), as it receives two unequal high tides and two unequal low tides per day. Tidal range was ~ 2m during the three measured spring tides and ~1m during the two measured neap tides. Root mean square wave heights (Figure 9B) averaged ~ 0.4m. However energy from several distant storms arrived at the beach during the experiment as indicated by extended periods of higher wave height. In the absence of the storm energy a low elevation background swell was the predominant wave feature. Shorter wave periods of 8–10s were associated with waves from the distant storms while 12–14s periods were measured with the background swell (Figure 9C).

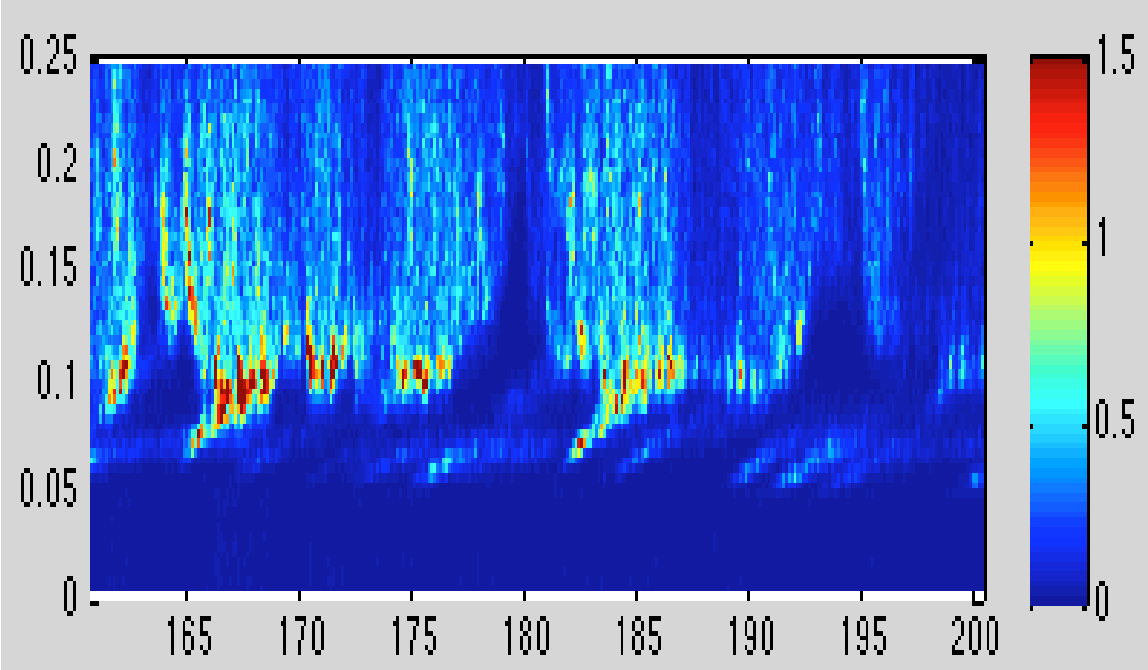

Figure 10. Hourly energy density spectra of onshore wave energy as a function of frequency and yearday. Energy color scale is plotted to the right.

Hourly onshore energy density spectra in the sea-swell band averaged hourly depicts the wave energy from distant storms arriving as swell at CRSB (Figure 10). Increased wave energy is visible as warmer colors centered near 0.1 Hz. Lower frequency waves arrive first and become progressively higher as expected from the dispersion relation. Examples of wave dispersion occur on year day 165 and 182. Background swell energy is visible near 0.06 Hz.

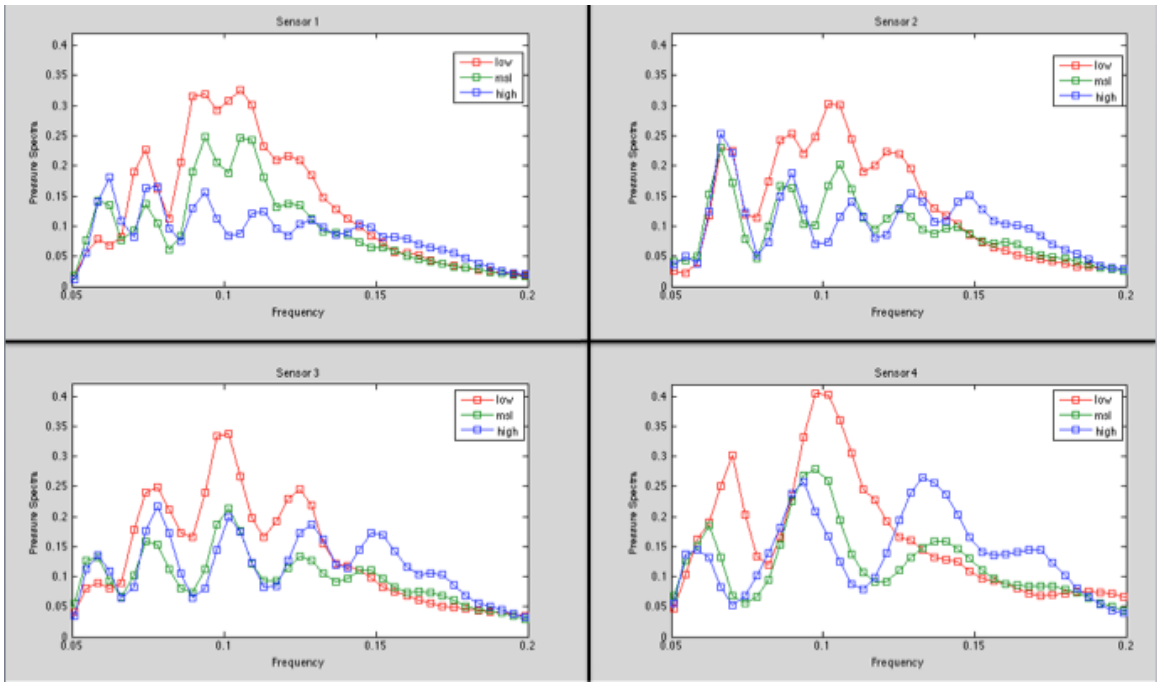

Figure 11. Measured nodal structure averaged by frequency for tides.

Pressure spectra averaged by tidal phase reveals changes to nodal structure with cross-shore distance along the array (Figure 11). Dips indicate location of nodes and peaks indicate anti-nodes. Nodes never reach the point of zero suggesting partial reflection is occurring, as a value of zero would indicate 100% reflection. Sensors farther offshore measured more nodes and anti-nodes. Changes in location and amplitude of nodes during low tide are related to changes of the tidal water level excursion.

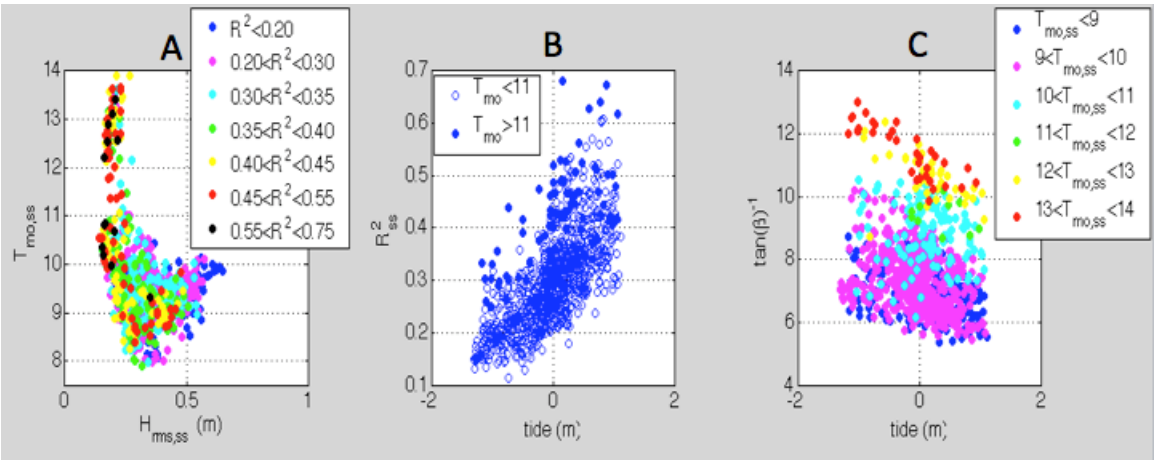

Figure 12. A) R^2 as a function of H (m) and T (s), where colors represent R^2 values. B) R^2 as a function of tides. Dashed line represents linear regression for T_{mo} (wave period)<11. C) Battjes (1974) equation solved for beach slope, where colors represent T_{mo} .

Batjjes (1974) relationship suggests that long period small waves are more reflective than short period or large wave heights, assuming a constant slope. We tested this idea with the CRSB data set (Figure 12A). The general trend supports Battjes (1974) relationship. T_{mo}> 12 saw the highest observed R^2 values approaching 80% while T_{mo}< 8 observed values of 20–30 %. Lowest wave elevations coincided with the highest observed R^2 while the absolute lowest observed values of <20% occurred during the tallest waves.

Elgar et al. (1994) and Miles and Russell (2001) observed higher R^2 values during high tide. Plotting R^2 against tide (Figure 12 B) for CRSB supports the previous findings with higher values measured at high tide. The data plot follows a linear trend in R^2 values for T_{mo}<11. These results were not expected due to the uniform nearshore slope at CRSB. Onshore energy density plots show a peak at around 0.10 Hz during low tide and near MSL (Figure 13 top panels). During high tide the energy peak is measured at a higher frequency of 0.15 Hz. This increase at higher frequency, during high tide, was observed at all sensor locations and may account for the higher R^2 values at high tide (Figure 12B).

Battjes (1974) equation for wave reflection (Eq. 3) expressed for beach slope is utilized to determine the location on the beach slope where waves are reflected. Results are sorted by wave period and slope is represented by $\tan\beta^{-1}$. The steep nearshore slope of 1/7.6 reflected waves with shorter periods, while waves with longer periods were reflected farther offshore on the more gradual slope (Figure 12 C).

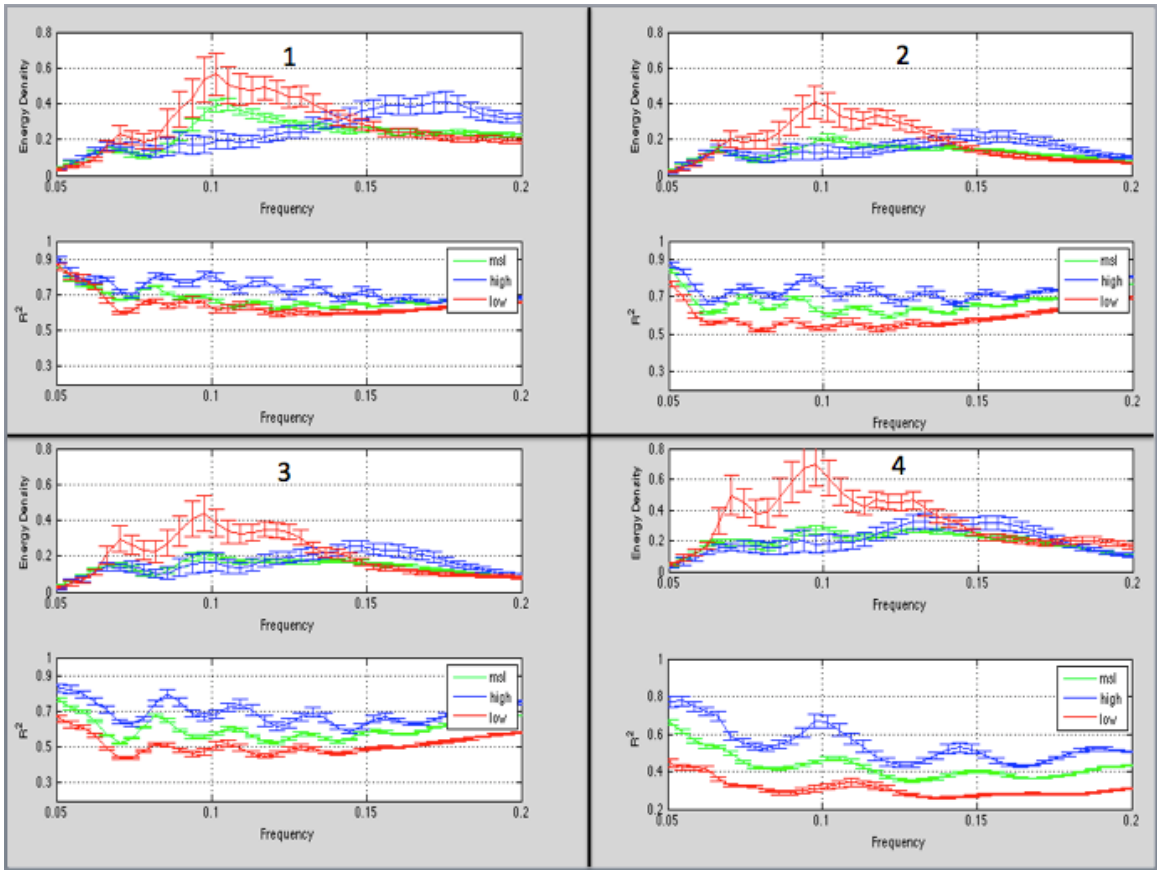

Figure 13. Quad panel of averaged onshore energy density (upper panel) and averaged R^2 in frequency for sensors 1–4.

Higher R^2 values, in the sea swell band, were measured at lower frequencies and decreased moving toward higher frequencies (Figure 13). This suggests that R^2 is frequency dependant. The highest values for R^2 measured during high tide.

IV. MODEL COMPARISON

A. MODEL OVERVIEW

Observed data were compared to output from an analytical model of reflective wave energy on a two-slope beach. Hotta et al. (1981) developed the model applying contributions from previous research by Lamb (1932), Friedrichs (1948), Carrier and Greenspan (1958), Carrier (1966) and Suhayda (1974). Through theoretical research Lamb (1932) solved linear long wave equations for a sloping beach accounting for tides. His results were expressed as zero-order Bessel functions of the first kind (J_0). Friedrichs (1948) research provided solutions for linear small amplitude wave equations at any depth on a sloping beach. As he moved closer to the shoreline his solutions became the tidal solution which were expressed as zero-order Bessel functions. Carrier and Greenspan (1958) obtained explicit solutions for non-linear shallow water equations. Solutions were expressed as zero order Bessel functions. Carrier (1966), building on his work with Greenspan, investigated gravity waves as they propagate over a complicated bottom using the non-linear shallow water equations.

Suhayda (1974) used the solution obtained by Lamb during his research while investigating standing waves on a smooth, steep sloping beach. He was interested in solving for reflection on beaches composed of two slopes. His expression was written for both slopes individually then solutions were matched at the slope break (Eq. 4 and 5).

Refining the Suhayda (1974) equation, Hotta et al. (1981) started by using the two-dimensional linear long wave equations. The origin of the coordinate system is the intersection point of the still water level and the sloping bottom (Figure14). Energy is assumed to arrive normal to the shoreline ensuring specular reflection. Beginning with the two-dimensional linear long wave equation,

$$\frac{\partial n}{\partial t} + \frac{\partial}{\partial x}(uh) = 0 \qquad (9)$$

$$\frac{\partial u}{\partial t} + g\frac{\partial \eta}{\partial x} = 0\,, \tag{10}$$

where η=η (*x*, *t*) is the sea surface elevation, $u = (x,t)$ is the horizontal component of the onshore water velocity and h=h (*x*) is the water depth at cross shore location x.

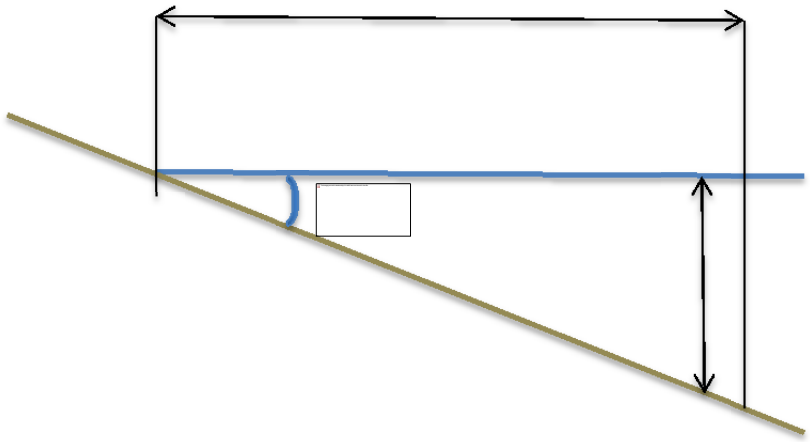

Figure 14. Coordinate system for a one-slope beach.

Cross-differentiating Eqs. 10 and 11 yields Eqs. 12 and 13 respectively;

$$\frac{\partial^2 \eta}{\partial x^2} + \frac{\tan\beta}{h}\frac{\partial \eta}{dx} - \frac{1}{gh}\frac{\partial^2 \eta}{\partial t^2} = 0 \tag{11}$$

,

$$h\frac{\partial^2 u}{\partial x^2} + 2\tan\beta\frac{\partial u}{\partial x} - \frac{1}{g}\frac{\partial^2 u}{\partial t^2} = 0 \tag{12}$$

,

where $\tan\beta = -\frac{\partial h}{\partial x}$ is the bottom slope. If we assume

$$\eta(x,t) = \bar{\eta}(x)e^{i\sigma t} \tag{13}$$

$$u(x,t) = \bar{u}(x)e^{i\sigma t} \tag{14}$$

Eqs. 11 and 12 become,

$$\bar{\eta}'' + \frac{1}{x}\bar{\eta}' + \frac{\sigma^2}{g\tan\beta x}\bar{\eta} = 0 \tag{15}$$

$$\bar{u}'' + \frac{2}{x}\bar{u}' + \frac{\sigma^2}{g\tan\beta x}\bar{u} = 0\,. \tag{16}$$

Since there is only one independent variable in each equation the partial differential operator, ∂, can be changed to the ordinary differential operator, d. Transforming the independent variable to $\xi = x^{\frac{1}{2}}$, Eq. 15 becomes,

$$\frac{d^2\bar{\eta}}{d\xi^2} + \frac{1}{\xi}\frac{d\bar{\eta}}{d\xi} + \frac{4\sigma}{g\tan\beta}\bar{\eta} = 0 \tag{17}$$

Substituting $m^2 = 4\sigma^2 / g\tan\beta$ and $\xi_0 = m\xi$, Eq. 17 becomes,

$$\frac{d^2\bar{\eta}}{d\xi_0^2} + \frac{1}{\xi_0}\frac{d\bar{\eta}}{d\xi_0} + \bar{\eta} = 0 \tag{18}$$

where Eq. 18 is a zero order Bessel equation with the general solution given in terms of Bessel as,

$$\bar{\eta} = aJ_0\left(2\sigma\sqrt{\frac{x}{g\tan\beta}}\right) + bY_0\left(2\sigma\sqrt{\frac{x}{g\tan\beta}}\right)\quad, \tag{19}$$

where a and b are coefficients having the dimensions of length which are to be determined by the boundary conditions.

Inserting Eq. 14 into Eq. 10, we get,

$$\bar{u}(x) = i\frac{g}{\sigma}\frac{d\eta}{dx}\,,$$

and, therefore,

$$\bar{u}(x) = -i\sqrt{\frac{g}{\tan\beta x}}\left[aJ_1\left(2\sigma\sqrt{\frac{x}{g\tan\beta}}\right) + bY_1\left(2\sigma\sqrt{\frac{x}{g\tan\beta}}\right)\right] \tag{20}$$

because $Y_0 \Rightarrow\infty$ as $x_1 \Rightarrow 0$, the coefficient b must be set to zero for a solution describing the region of the origin. Eq. 20 can also be derived directly from Eqs. 12 and 14.

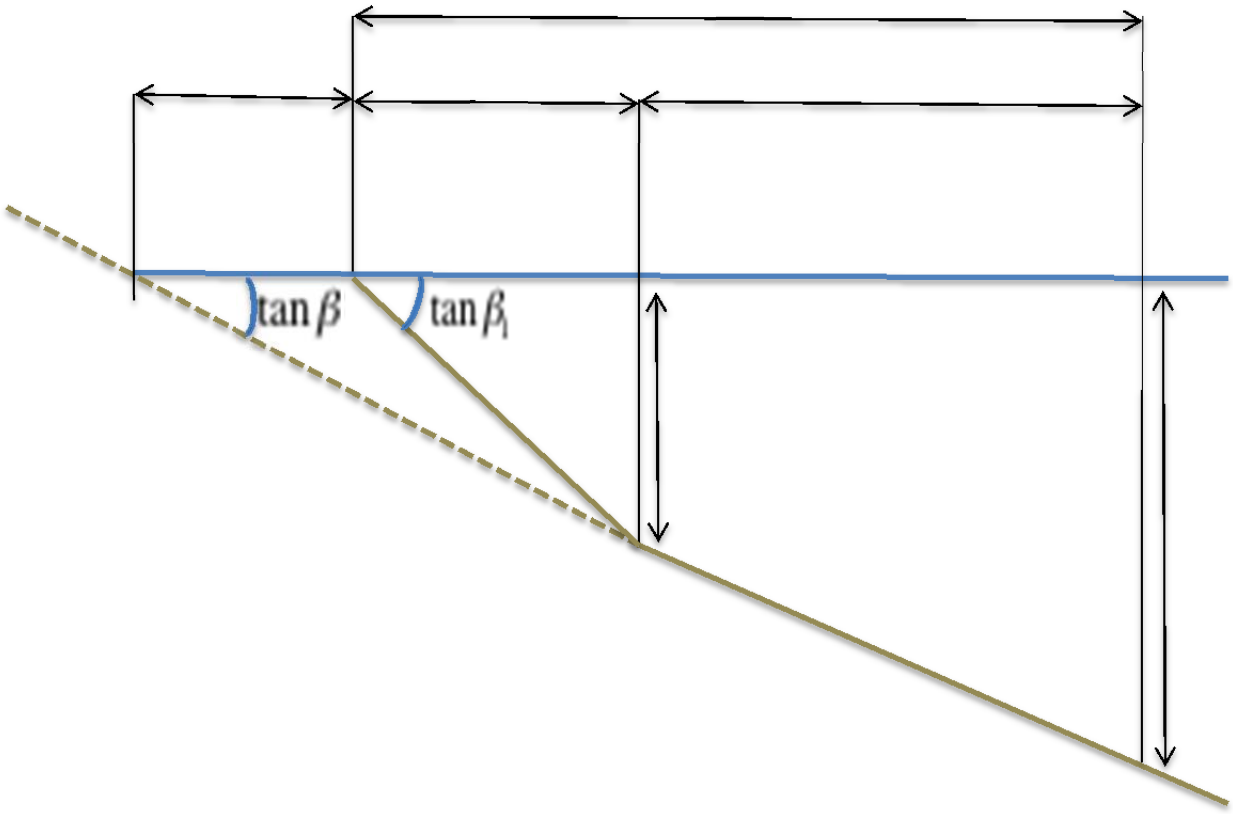

Figure 15. Coordinate system for a two-slope beach.

Starting with the steeper nearshore slope.

$0 \le x \le x_1$

$$\bar{n} = a_1 J_0\left(2\sigma\sqrt{\frac{x}{\tan\beta_1}}\right) \tag{21}$$

$$\bar{u} = -ia_1\sqrt{\frac{g}{x\tan\beta_1}}J_1\left(2\sigma\sqrt{\frac{x}{g\tan\beta_1}}\right) \tag{22}$$

,

The second half of the equation solves for the offshore slope (Figure 15).

$$x_1 < x$$

Where,

$$\overline{\eta} = a_2 J_0\left(2\sigma\sqrt{\frac{x+x_0}{g\tan\beta_2}}\right) + b_2 Y_0\left(2\sigma\sqrt{\frac{x+x_0}{g\tan\beta_2}}\right), \tag{23}$$

and

$$\overline{u} = -i\sqrt{\frac{g}{\tan\beta_2\left(x+x_0\right)}}\left[a_2 J_1\left(2\sigma\sqrt{\frac{x+x_0}{g\tan\beta_2}}\right) + b_2 Y_1\left(2\sigma\sqrt{\frac{x+x_0}{g\tan\beta_2}}\right)\right]. \tag{24}$$

Since the model requires solutions be equal at the slope break setting Eq. 21 equal to 23 and 22 equal to 24 we have,

$$a_1 J_0\left(2\sigma\sqrt{\frac{x_1}{g\tan\beta}}\right) = a_2 J_0\left(2\sigma\sqrt{\frac{x_1+x_0}{g\tan\beta}}\right) + b_2 Y_0\left(2\sigma\sqrt{\frac{x_1+x_0}{g\tan\beta}}\right),$$

$$a_1\sqrt{\frac{1}{\tan\beta_1 x_1}}J_1\left(2\sigma\sqrt{\frac{x_1}{g\tan\beta_1}}\right) = \sqrt{\frac{1}{\left(x_1+x_0\right)\tan\beta_2}}\left[a_2 J_1\left(2\sigma\sqrt{\frac{x_1+x_0}{g\tan\beta_2}}\right) + b_2 Y_0\left(\sqrt{\frac{x_1+x_0}{g\tan\beta_2}}\right)\right]$$

.

Since $x_1\tan\beta_1 = h_1$, and $\left(x+x_0\right)\tan\beta_2 = h_1$, the final solution is,

$$a_1 J_0\left(\frac{2\sigma}{\tan\beta_1}\sqrt{\frac{h_1}{g}}\right) = a_2 J_0\left(\frac{2\sigma}{\tan\beta_2}\sqrt{\frac{h_1}{g}}\right) + b_2 Y_0\left(\frac{2\sigma}{\tan\beta_2}\sqrt{\frac{h_1}{g}}\right), \tag{25}$$

$$a_1 J_1\left(\frac{2\sigma}{\tan\beta_1}\sqrt{\frac{h_1}{g}}\right) = a_2 J_1\left(\frac{2\sigma}{\tan\beta_2}\sqrt{\frac{h_1}{g}}\right) + b_2 Y_1\left(\frac{2\sigma}{\tan\beta_2}\sqrt{\frac{h_1}{g}}\right). \tag{26}$$

B. MODEL VALIDATION

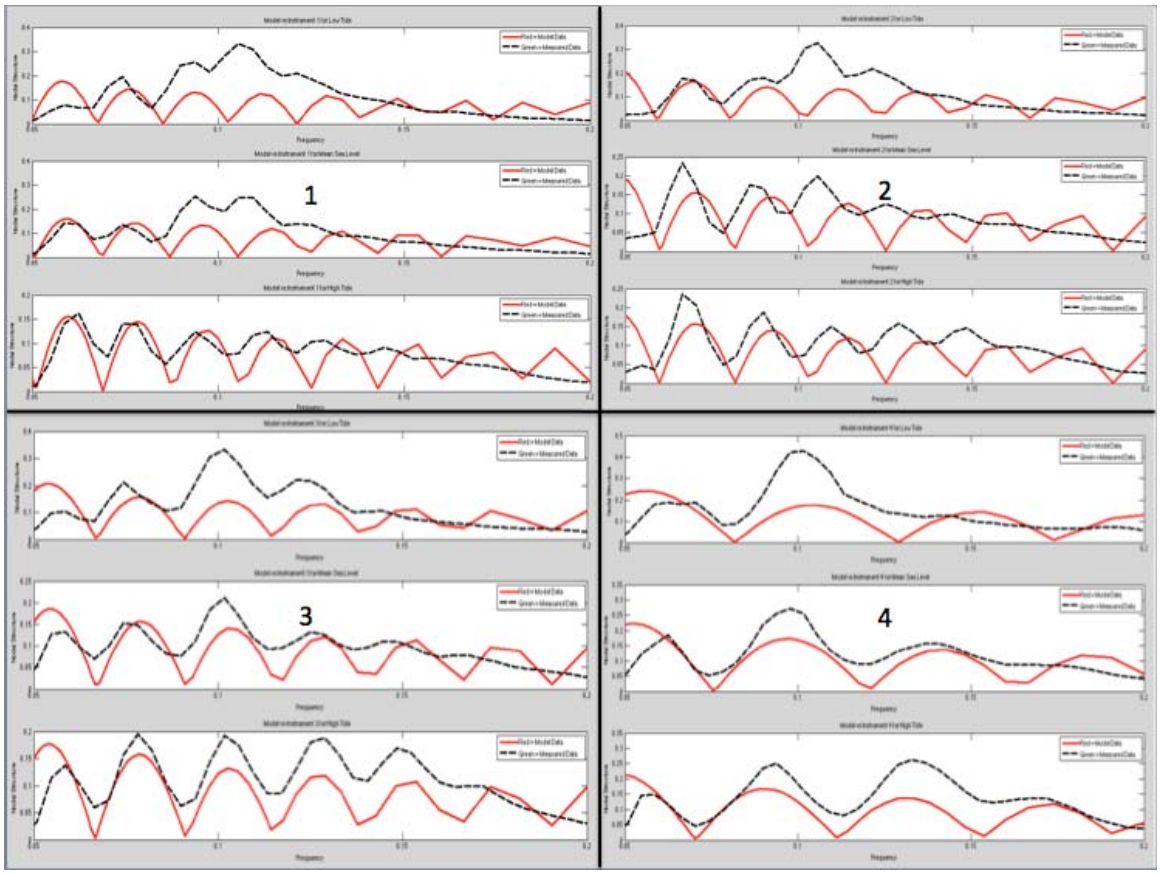

Figure 16. Measured (dashed black) versus predicted (red) nodal structure of reflected wave energy in the sea-swell frequency band for sensors 1–4. Top panel is high tide, center is MSL, and bottom is low tide.

Measured nodes and anti-nodes in the sea-swell frequency band were plotted against predicted nodal structure utilizing the analytical 2-slope model (Figure 16). The goal of the model is to determine the location of nodes and anti-nodes not actual amplitudes. Measured data collected at CRSB were used to validate the model results. Model runs were made for 100 different slopes between 1/3 and 1/19 for all tides to evaluate which slope produced the best fit to measured data. Results indicate that the steep 1/7.6 nearshore slope was primarily responsible for reflecting the wave energy.

The predicted location of the nodes (dips) and anti-nodes (peaks) were in good agreement with measured data. More nodes at higher frequencies and farther off shore were predicted, which is in agreement with observed conditions at CRSB.

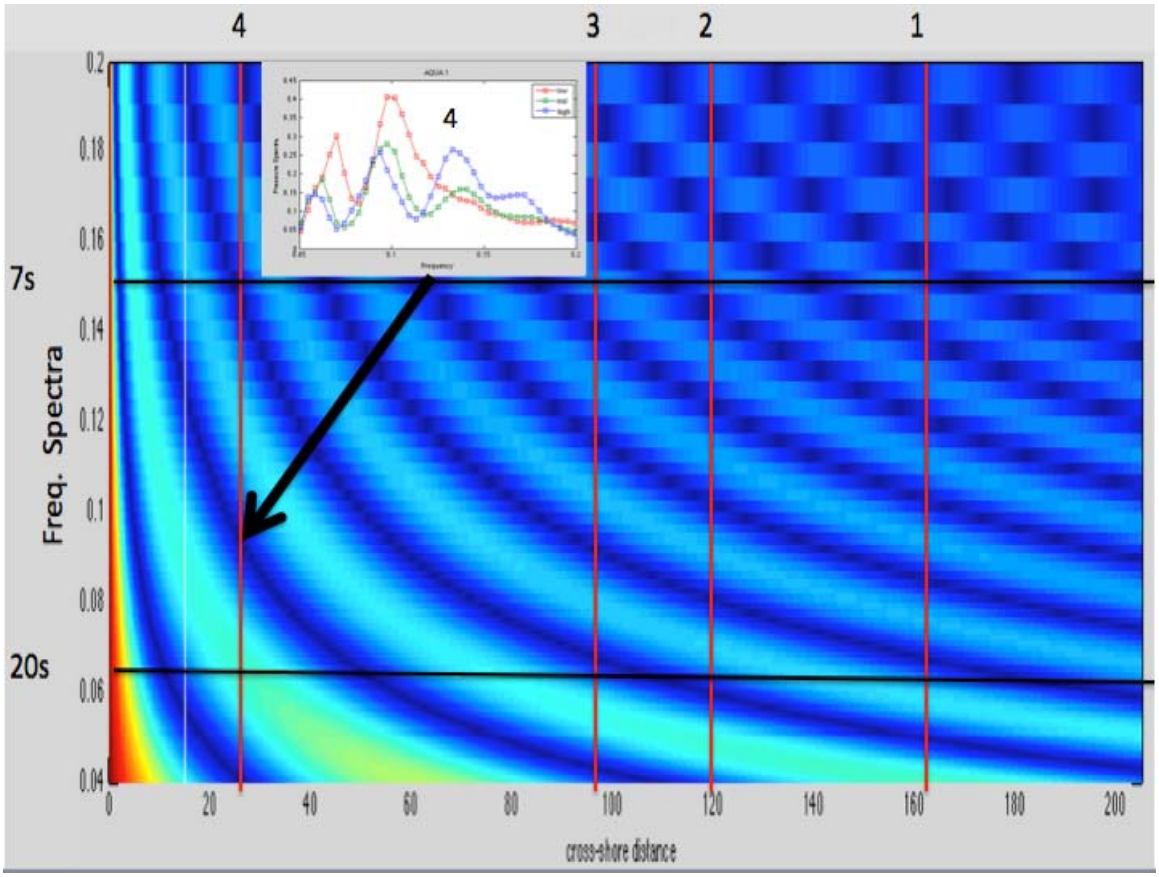

Figure 17. Predicted frequency spectra in sea swell frequency band in the cross-shore. Inset is measured nodal structure averaged over tides. Red vertical lines indicate sensor locations the white line marks the slope break. Warmer colors correspond to anti-nodes.

Predicted frequency spectra in the cross-shore showing nodal structure by frequency at each sensor location (Figure 17). Looking vertically at sensor 4 there is an anti-node for a 20s wave period but a node for a 7s period. This illustrates the complex nodal structure caused by waves of multiple frequencies present at CRSB. Comparing the model with measured nodal structure averaged by frequency for tides, predicted locations of nodes and anti-nodes are also in good agreement at all sensor locations

(sensor 4 shown). The general exception was during low tide when wave refraction caused a shift in nodal location. Waves with a 20s period produce two anti-nodes and one node between the shore and sensor 4. A wave with a 7 second period will produce 3 anti-nodes and two nodes in the distance. The increase in the number of nodes at higher frequency is in agreement with measured data.

V. SUMMARY AND CONCLUSION

Wave reflection from a steep natural beach was studied using measurements from a cross-shore line array of velocity profilers at CRSB, Carmel, CA. CRSB is a two-slope steep beach composed of a very steep nearshore slope of 1/7.6 and an offshore slope of 1/19. The beach features a very steep, but narrow, step of 1/3 at the slope break and does not have a sub aqueous sand bar. Field data were utilized to validate an analytical two-slope model to predict the cross-shore standing wave structure. The impacts of tides and sensitivities to beach slopes were studied. The predicted nodal structure from the model was in good agreement with the CRSB dataset. Analysis of model output for various slope angles from 1/3 to 1/19 showed the best representation of measured data was at 1/7.6 coinciding with the steep nearshore slope at CRSB. The model also reproduces the observed decrease in node spacing at higher frequency and farther offshore. Measurements showed highest R^2 during long period, low waves with values observed as high as 80%. Higher values of R^2 were observed at high tide. Although this agreed with previous studies (Elgar et al. (1994)) the results were unexpected since the slope at the nearshore did not change at high tide as in those studies. Energy density of onshore wave energy measured more energy at higher frequency (0.15Hz) during high tide. While the reason for this is uncertain it suggests the increase in R^2 is because more energy is available for reflection at high tide.

THIS PAGE INTENTIONALLY LEFT BLANK

LIST OF REFERENCES

Battjes, J.A., 1974. "Surf Similarity." *Coastal Engineering,* Vol. 1, 466–479.

Carrier, G.F. and H.P. Greenspan, 1958. "Water waves of finite amplitude on a sloping beach." *Journal Fluid Mech. 4 (Part 1).* 97–109.

Carrier, G.F., 1966. "Gravity waves on water of variable depth." *Journal Fluid Mech. 24(Part 4)*. 644–659.

Ching-Piao Tsai, Hong-Bin Chen, Hwung-Hweng Hwung, and Ming-Jen Huang. 2004 "Examination of empirical formulas for wave shoaling and breaking on steep slopes." *Ocean Engineering 32 (2005).* 469–483.

Elgar, S., Herbers T.H.C., and Guza, R.T., 1994. "Reflection of ocean surface gravity waves from a natural beach." *Journal Physical Oceanography*, 24(7), 1503–1511.

Friedrichs, K.O., 1948. "Water waves on a shallow sloping beach." *Communications on Pure and Applied. Math 1*, 109–134.

Hotta, H., Mizuguchi, M., and Isobe, M., 1981. "Observations of long period waves in the nearshore zone." *Coastal Engineering in Japan*, Vol. 24, 41–76.

Huntley, D.A., Simmonds, D. and Tatavarti, R., 1999. "Use of Collocated Sensors to Measure Coastal Wave Reflection." *Journal of Waterway, Port, Coastal, and Ocean Engineering*, Vol. 125, No.1, 46–62.

Iribarren, C.R. and Nogales, C., 1949. "Protection des ports." *Section 2, Comm. 4, XXIIth Int. Nav. Congress, Lisbon*, 31–80.

Komar, P.D., 1998. "Beach Processes and Sedimentation." *Prentice Hall 2nd Edition*.

Lamb, H., 1932. "Hydrodynamics." 6th edition. *Dover Publications*, 738.

Laudier, N.A. 2011. "Measured and modeled wave overtopping on a natural beach." *Coastal Engineering 58*, 815–825.

Miche, R., 1955. "Le pouvoir reflechissant des ouvrages maritimes exposes a l'action de la houle." *Ann. Points. Chaussees*, Vol. 121, 285–319.

Miles and Russell, 2004. "Dynamics of a reflective beach with a low tide terrace." *Continental Shelf Research*, Vol. 24, 1219–1247.

Neshaei, Holmes, and Salimi, 2009."A semi-empirical model for beach profile evolution in the vicinity of reflective structures." *Ocean Engineering,* Vol. 26, 1303–1315.

Reniers, Thornton, Stanton and Roelvink, 2004." Vertical flow structure during Sandy Duck: observations and modeling." *Coastal Engineering*, Vol. 51, 237–260.

Ruggiero, P., Holman, R.A., and Beach, R.A., 2004. "Wave run-up on a high-energy dissipative beach." *Journal of Geophysical Research*, Vol. 109, C06025, 1–12.

Sheremet, A., Guza, R. T., Elgar, S., and T. H. C. Herbers, 2001."Observation of nearshore infragravity waves: Seaward and shoreward propagating components." *J. of Geophysical Research*, Vol. 107, No. C8, 2002, 1–10.

Short, 1999. "Handbook of Beach and Shoreface Morphodynamics." John Wiley and Sons Ltd.

Suhayda, J. N., 1974. "Standing Waves on Beaches." *Journal of Geophysical Research*, Vol. 79, No.21, 3065–3071.

Tatavarti, R.S.V.N., Huntley, D.A. and Bowen, A.J. 1988. "Incoming and outgoing wave interactions on beaches." *Proc. 21st Conf. On Coastal Eng.*, American Soc. Civil Eng., New York, NY. 1104–1120.

INITIAL DISTRIBUTION LIST

1. Defense Technical Information Center
   Ft. Belvoir, Virginia

2. Dudley Knox Library
   Naval Postgraduate School
   Monterey, California

3. Professor Jamie MacMahan
   Naval Postgraduate School
   Monterey, California

4. Professor Thomas Herbers
   Naval Postgraduate School
   Monterey, California

5. Professor Jeffrey Paduan
   Naval Postgraduate School
   Monterey, California